An afferent subcortical white matter pathway to the amygdala facilitates fear recognition

Jessica McFadyen[1,2], Jason B. Mattingley[1,3], & Marta I. Garrido[1,2,4,5]*

[1]Queensland Brain Institute, University of Queensland, Brisbane, QLD 4072 Australia
[2]Australian Research Council of Excellence for Integrative Brain Function, Australia
[3]School of Psychology, University of Queensland, Brisbane, QLD 4072 Australia
[4]School of Mathematics and Physics, University of Queensland, Brisbane, QLD 4072 Australia
[5]Centre for Advanced Imaging, University of Queensland, Brisbane, QLD 4072 Australia
* corresponding author: j.mcfadyen@uq.edu.au

Abstract

Our ability to rapidly detect threats is thought to be subserved by a subcortical pathway that quickly conveys visual information to the amygdala. This neural shortcut has been demonstrated in animals but has rarely been shown in the human brain. Importantly, it remains unclear whether such a pathway might influence neural activity and behaviour. We conducted a multimodal neuroimaging study of 622 participants from the Human Connectome Project. We applied probabilistic tractography to diffusion-weighted images, reconstructing a subcortical pathway to the amygdala from the superior colliculus via the pulvinar. We then computationally modelled the flow of neural activity during a face-viewing task and found strong evidence for a functionally-afferent subcortical pathway. Critically, individuals with greater fibre density in this pathway also had stronger dynamic coupling and enhanced fearful face recognition. Our findings provide converging evidence for the recruitment of an afferent subcortical route to the amygdala in the human brain that facilitates fear recognition.

Keywords: amygdala, pulvinar, faces, tractography, diffusion, fMRI, dynamic causal modelling

Introduction

Decades ago, rodent research uncovered a subcortical pathway to the amygdala that rapidly transmits auditory signals of threat even when the auditory cortex is destroyed[1]. Since this discovery, researchers have sought an equivalent visual pathway that might explain how it is that people with a lesioned primary visual cortex can still respond to affective visual stimuli that they cannot consciously see[2]. The superior colliculus, pulvinar, and amygdala have been identified as nodes of a human subcortical route to the amygdala that bypasses the cortex[3]. These subcortical areas consistently coactivate in cortically blind patients[4, 5] (as well as in healthy adults[3, 6, 7]) when they view emotional stimuli, such as angry or fearful faces. Magnetoencephalography studies using computational modelling have investigated whether the activation of these subcortical nodes is causally related. These studies have consistently found evidence for a forward connection between the pulvinar and amygdala[8-10]. The dynamic causal relationship between the superior colliculus and the pulvinar, however, remains unexplored in the human brain[11]. The pulvinar also has several functional and cytoarchitectural subregions[12] and it is unclear how these connect to the superior colliculus and the amygdala and what roles these subregions may play in mediating transmission along the subcortical route[13, 14]. As such, the hypothesis that the subcortical route rapidly transfers information from the retina to the amygdala without interference has been heavily criticised[14, 15]. Furthermore, the pulvinar is highly connected with a widespread network of cortical regions that may contribute to transmission along the

subcortical route[16, 17]. Hence, it remains unknown whether the functional activation of the human superior colliculus, pulvinar and amygdala during affective processing bears any relation to an underlying structural pathway[14].

Recent animal research has revealed several potential direct subcortical pathways that have a causal relationship with fearful behaviour in response to visual threats[18-20]. In the absence of relevant post-mortem human research, however, our anatomical knowledge of the human subcortical route to the amygdala can only be derived from tractography of diffusion-weighted images (DWI). Tamietto et al. (2012) examined DWIs from a blindsight patient whose left primary visual cortex was destroyed. The white matter structure of the subcortical route was estimated for the patient and for six healthy, age-matched controls. Critically, the subcortical route had greater fractional anisotropy in the patient's damaged hemisphere, suggesting a neuroplastic increase in myelination to compensate for the disrupted cortical pathways[21]. In a similar study, Rafal et al. (2015) used tractography to investigate the subcortical route in 20 healthy humans and 8 macaques. The subcortical route was reconstructed in both hemispheres for 19 of the 20 human participants and 7 of the 8 macaques[22]. Notably, this sample of human participants was recently expanded and re-examined. Individuals with greater fractional anisotropy along the subcortical route also had a stronger bias toward threat when making saccades to scenes[13].

Diffusion tractography may grant insight into the strength of anatomical connectivity between regions but it cannot reveal the direction of information transfer, nor can it be used as direct evidence alone for the anatomical existence of a neural pathway. The anatomical presence and the direction-specific neural flow of emotional visual information along the subcortical route has never been concurrently investigated in humans to definitively show that the subcortical route is a direct, afferent pathway specifically associated with fear[14, 15]. Such a finding would have important implications for the very foundation of visual threat perception, given this pathway's potential for rapid information transfer[8, 23] and unconscious processing[2]. Here, we aimed to comprehensively investigate this putative amygdala pathway in a large sample of over 600 healthy human adults from the Human Connectome Project (HCP) dataset using a multimodal imaging approach to encompass structure, function and behaviour. First, we used DWI to reconstruct the subcortical route from the superior colliculus to the amygdala, via the pulvinar, and estimated its fibre density on an unprecedentedly large sample. We then examined whether this putative pathway targeted the same pulvinar functional subdivisions. Next, we modelled the direction-specific flow of neural activity for faces, testing whether a functional subcortical route is recruited to transmit information toward the amygdala. Finally, we asked whether the fibre density of the subcortical route predicts both fearful face recognition as well as the strength of dynamic coupling between the superior colliculus, pulvinar, and amygdala.

Results

Reconstructing the subcortical route using tractography

The first step in our investigation was to evaluate the evidence for an anatomical subcortical route to the amygdala in the healthy human brain. We exploited high-quality neuroimaging data from a large sample of 622 participants made available by the HCP[24]. We then reconstructed the white matter structure of the subcortical route using two complementary tractography methods for cross-validation. We began with global tractography, a Bayesian approach to reconstructing whole-brain fibre configurations that best explain DWI data (see **Online Methods** for details). We discovered that the superior colliculus (SC) was connected to the pulvinar (fibre counts for PUL; left: M = 13.23, SD = 5.56, right: M = 13.00, SD = 5.59, minimum of 2 fibres per participant). The pulvinar and the amygdala were also connected (fibre counts for left: M = 5.33, SD = 2.79, and right: M = 6.75, SD = 2.90), with most participants having at least one connecting fibre (zero fibres for left PUL-AMG for 8 participants – only 1.28% of total sample). Thus, this

relatively conservative method of fibre reconstruction (as it takes into account the entire brain) can reliably detect evidence for a subcortical route across a large sample of participants. We also found a hemispheric lateralisation, such that there were more reconstructed fibres for the right than the left PUL-AMG pathway ($F(1,617) = 39.865$, $p = 5.206 \times 10^{-10}$, $\eta_p^2 = .061$; $t(617) = -9.785$, $p = 4.070 \times 10^{-21}$).

To assess the validity of our findings we used a second tractography method, namely "local" probabilistic streamline tractography, as used by Rafal et al. (2015) to reconstruct the subcortical route to the amygdala[22]. We generated streamlines between our regions of interest (ROIs) and found that the superior colliculus connected to the pulvinar (streamline counts for left: $M = 1403.32$, $SD = 417.16$, right: $M = 111.59$, $SD = 358.60$, minimum of six streamlines per participant) and the pulvinar connected to the amygdala (left: $M = 575.42$, $SD = 203.03$, right: $M = 575.42$, $SD = 248.85$, minimum 66 streamlines per participant). To evaluate whether these streamlines counts were reconstructed significantly above chance, we compared the numbers with those produced by a null distribution algorithm, which essentially generated streamlines at random[25]. We found that the number of streamlines was significantly different from chance for each connection, as determined by a series of paired *t*-tests (see **Fig. 1**), suggesting that the DWI data produced meaningful streamlines between our ROIs.

We employed a recently developed method, SIFT2, which estimates the apparent fibre density of the streamlines connecting two regions of interest. This method more accurately represents the true underlying white matter structure[26]. The apparent fibre density of the streamlines generated using local tractography followed the same pattern as the global tractography fibre counts, such that there was greater fibre density for the SC-PUL connection (left: $M = 6.25$, $SEM = 0.09$, right: $M = 5.34$, $SEM = 0.07$) than the PUL-AMG connection (left: $M = 3.98$, $SEM = 0.05$, right: $M = 4.94$, $SEM = 0.06$, $F(1,608) = 257.135$, $p = 1.603 \times 10^{-48}$, $\eta_p^2 = .297$). Fibre density was also greater on the right than the left for the PUL-AMG connection ($t(608) = -18.205$, $p = 1.960 \times 10^{-59}$) but, additionally, we also observed greater fibre density for the left than right SC-PUL connection ($t(608) = 10.749$, $p = 8.600 \times 10^{-}25$, $F(1,608) = 401.417$, $p = 6.002 \times 10^{-69}$, $\eta_p^2 = .398$). Taken together, our tractography analyses provide strong convergent evidence for a subcortical white matter pathway to the amygdala in the human brain.

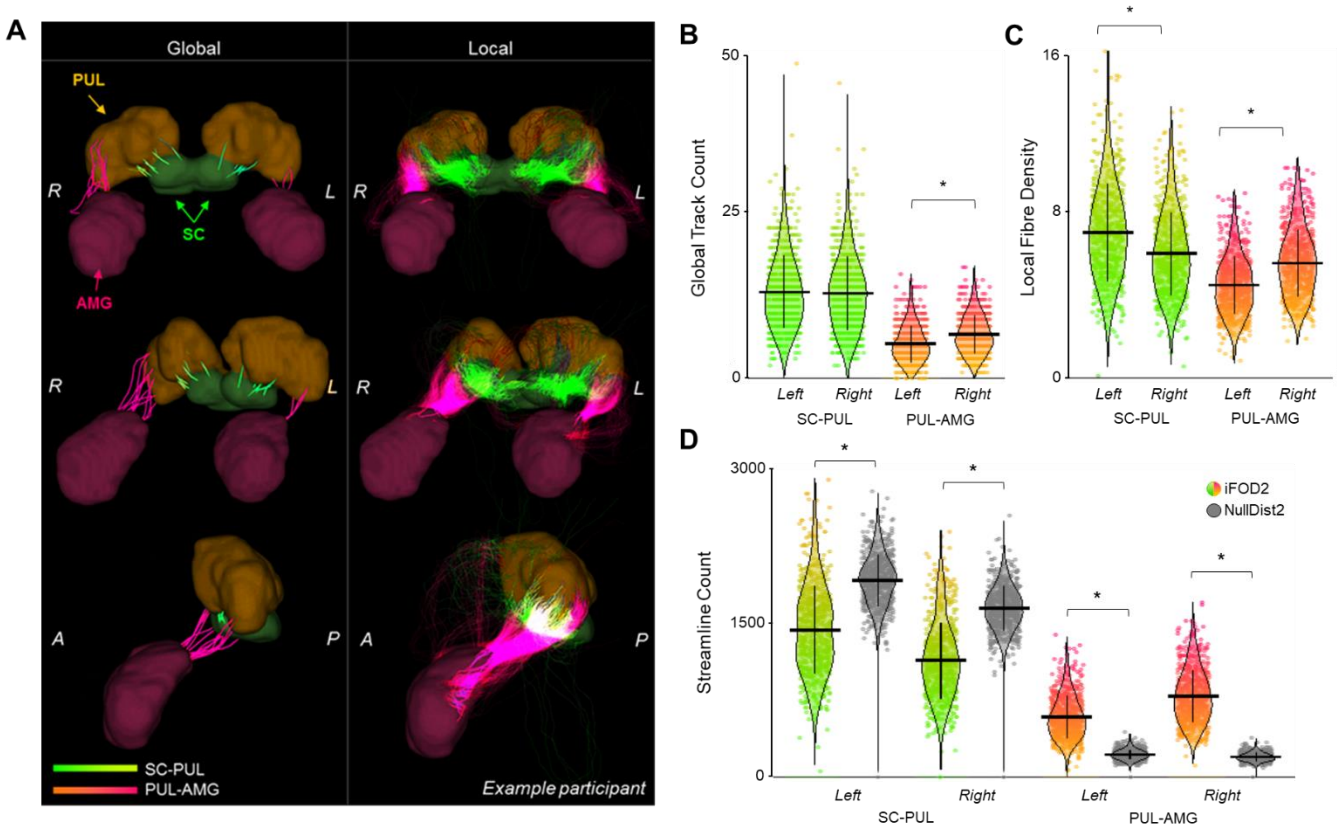

Figure 1. **Global and local probabilistic tractography reconstructions of the subcortical route to the amygdala. A)** The subcortical route reconstructed by global (left column) and local (right column) tractography in one example participant. Streamlines between the superior colliculus and pulvinar are green and streamlines between the pulvinar and amygdala are pink. The top row is a coronal section, the middle row is coronal section rotated 45° towards axial, and the bottom row is an axial section. Participant-specific ROIs have been 3D rendered. A = anterior, P = posterior, L = left, R = right. **B)** Dot plots of the global track count and **C)** local fibre density from all 622 participants. Horizontal lines indicate the mean, vertical black lines indicate one standard deviation. Density distribution is represented by each violin plot. * = $p < .05$ **D)** The streamline count of the local tractography is shown (green-yellow for SC-PUL, orange-pink for PUL-AMG) compared with the streamline count generated by a null distribution (grey). * = $p_{FDR} < .05$

A direct route through the right inferior pulvinar

We have replicated evidence for a subcortical white matter route to the amygdala from the superior colliculus via the pulvinar using multiple methods for cross-validation in an unprecedented sample over 30 times larger than previous studies[13, 21, 22]. However, it remains unknown whether this functions as a continuous pathway[14]. This is critical because the pulvinar is highly connected with the visual, temporal, parietal, and frontal cortices[16] and thus may simply mediate communication between these areas and the amygdala, rather than enable a direct route for rapid fear processing. To investigate this, we asked whether the two halves of the subcortical route (i.e. SC-PUL and PUL-AMG) connected to the *same* subregion of the pulvinar. This would serve as the fastest and thus most direct path from the superior colliculus to the amygdala. To answer this question, we investigated whether the connectivity strength to and from the same pulvinar subregion (from the superior colliculus and to the amygdala, respectively) were positively correlated, which would suggest the concurrent use of that white matter pathway.

We used a parcellated pulvinar mask generated by a previous meta-analysis of functional co-activation[12] that maps closely onto the pulvinar's cytoarchitecture[27]. We then repeated the initial tractography analysis but instead of using one pulvinar region of interest (i.e., target) we used five pulvinar subregions: inferior, superior, anterior, medial, and lateral (see **Fig. 2A**). We then correlated the fibre density measures (from

both local and global tractography) between each pulvinar subregion-specific SC-PUL and PUL-AMG pathway (see **Online Methods** for details of principal components analysis which was used to extract the unique variance per subregion-specific pathway), resulting in a total of 100 Pearson's correlations. This revealed several significant relationships between subregion-specific pathways, many of which were between pathways that connected to *different* pulvinar subregions (see **Fig. 2C**, off-diagonal matrix entries). Critically, however, the *right inferior pulvinar* was the only subregion to show a significant positive relationship with both the superior colliculus and amygdala for both global *and* local tractography methods for the *same* pulvinar subregion (global: $r = .137$, $p_{bonf} = .030$, local: $r = .188$, $p_{bonf} = 2.982 \times 10^{-6}$, see **Fig. 2C** – diagonal matrix entries). No other relationships were consistent and significant across both methods for the *same* pulvinar subregion. The inferior pulvinar also had the strongest fibre density for connections to the amygdala and was also one of the strongest subregions to connect to the superior colliculus. Thus, while there were many connections that correlated across pulvinar subregions, these relationships were not consistent across tractography methods. Therefore, the mutual connections with the inferior pulvinar observed for both tractography methods provided the strongest evidence for a direct pathway from the superior colliculus to the amygdala.

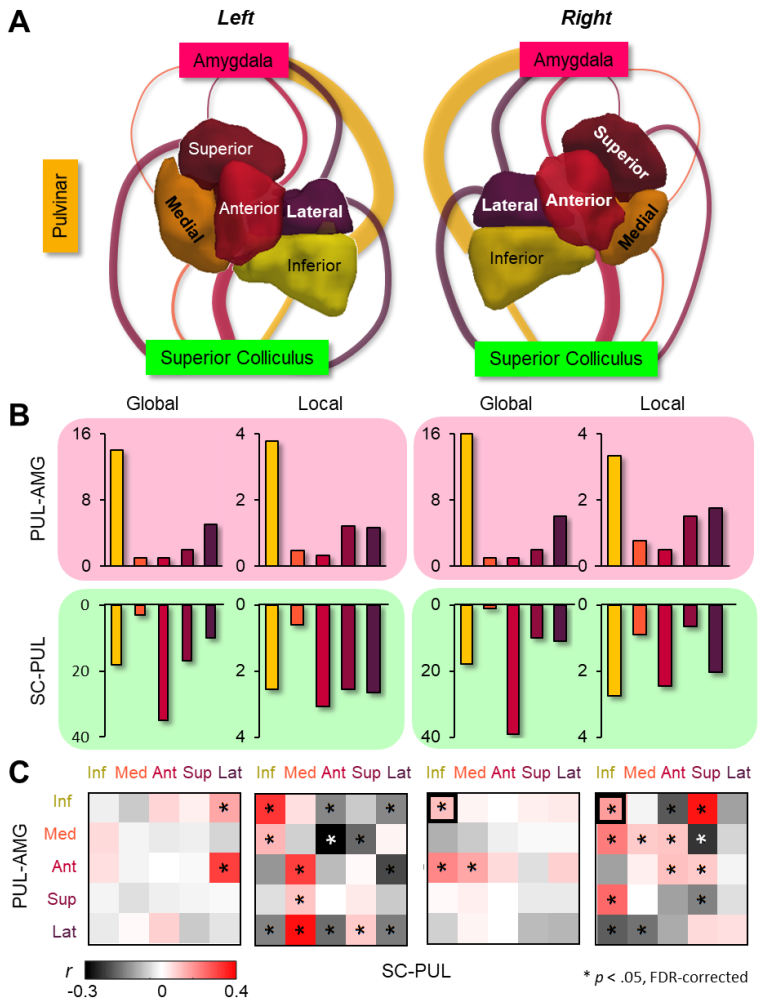

Figure 2. **Connectivity between pulvinar subregions and the superior colliculus and the amygdala**. Results from left and right hemispheres are shown in the left and right columns, respectively, for both global and local tractography methods. **A)** 3D renders of the pulvinar subregions with lines representing connections to the superior colliculus (top) and the amygdala (bottom). The thickness of the lines indicates connectivity strength, relative to connectivity between other subregions and that region. **B)** Global track counts and local summed weights for the PUL-AMG (pink box) and SC-PUL (green box) connections. The five subregions are colour-coded as per the 3D renders in A). **C)** Asterisks indicate significant correlations ($p_{FDR} < .05$) between the

subregion-specific connection strength of the SC-PUL (columns) and PUL-AMG (rows) pathways. Diagonal matrix entries correspond to the correlation of white matter pathways linking superior colliculus and the amygdala via the *same* pulvinar subregion, suggesting a continuous pathway from the superior colliculus to the amygdala. Off-diagonal matrix entries correspond to pathways linking superior colliculus and the amygdala via *different* pulvinar subregions. Red indicates the strength of positive correlations and black indicates the strength of negative correlations, where the magnitude of Pearson's *r* is indicated by the colour bar. The key finding is highlighted by two black boxes, showing that the connections between the inferior pulvinar and the superior colliculus and amygdala were significantly positively correlated for both global and local tractography.

Greater fibre density predicts better fearful face perception

We wanted to translate our work in humans to animal research that has demonstrated clear relationships between the anatomical presence of a subcortical route and fearful behaviour[18-20]. To this end, we examined data from the Penn Emotion Recognition task, which was implemented in the HCP battery of behavioural tests. Note that this task was different from the behavioural task used in the fMRI experiment. In this task, participants were serially presented with 40 faces that were either happy, sad, angry, fearful, or neutral. Participants were most accurate with identifying the emotional expression of happy faces (M = 7.96, SD = 0.21), followed by neutral (M = 7.22, SD = 1.18), and then fearful faces (M = 7.02, SD = 1.03). Recognition was poorest for angry (M = 6.86, SD = 0.98) and sad faces (M = 6.82, SD = 1.12).

We then investigated the association between these scores (see **Fig. A**) with the fibre density of the subcortical route. We chose not to include happy or neutral expressions in our analysis because the data were substantially negatively skewed (skewness for: happy = -5.821; neutral = -2.053; angry = -0.719; fearful = -1.188; sad = -1.090). Thus, we entered the global and local fibre density measures for the SC-PUL and PUL-AMG pathways into a multivariate regression with recognition accuracy scores for fearful, angry, and sad faces as covariates (we excluded 25 outliers, 4.02% of sample, with a Cook's distance of more than 3 SDs from the mean). Overall, there was a significant multivariate relationship between tractography and recognition accuracy for fearful faces ($F(8, 585) = 2.100$, $p = .034$, Wilk's $\Lambda = .972$, $n_p^2 = .028$; see **Fig. B**). This was driven predominantly by fibre density of the left ($F(1,592) = 12.213$, $p = .001$, $n_p^2 = .020$) and right ($F(1,592) = 8.915$, $p = .003$, $n_p^2 = .015$) PUL-AMG connections' local fibre density. These results suggest that the fibre density of the subcortical route is associated with fearful face recognition more so than with other negative (sad) or threatening (angry) emotional expressions.

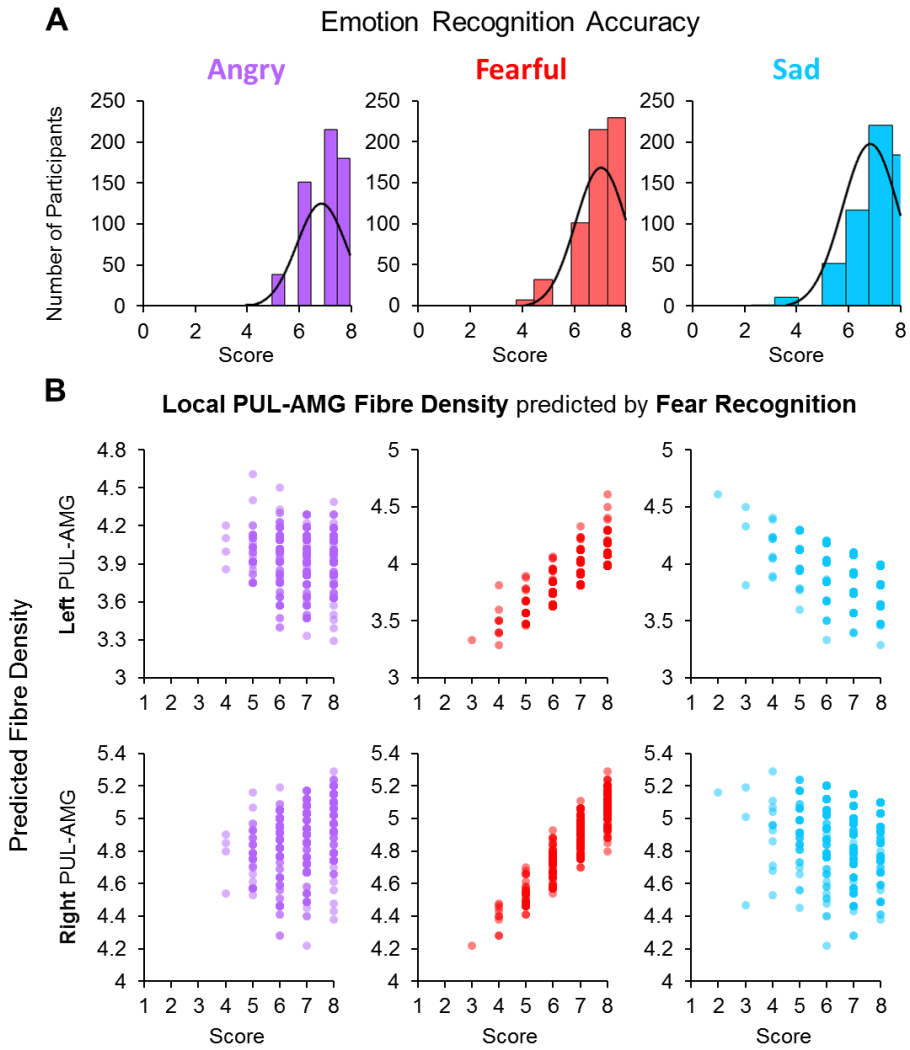

Figure 3. Relationship between behavioural performance and tractography. A) Histograms of scores (out of eight) for correctly recognising the emotional expression of angry, fearful, and sad faces from the Penn Recognition Test. Normal distribution function is plotted. **B)** The relationships between recognition of angry (purple), fearful (red), and sad (blue) faces (*x*-axes) and the left (top row) and right (bottom row) local fibre density of the PUL-AMG connection (*y*-axes) produced by a multivariate regression. Fearful face recognition accuracy was significantly related to local fibre density for the left and right PUL-AMG connections.

Subcortical and cortical BOLD signal to emotional faces

We used dynamic causal modelling to infer the dynamic (or effective) connectivity between each node of the subcortical route and determine the directionality of the functional interactions occurring along the anatomical pathway mapping described above. First, it was necessary to establish any differences in functional activation within these nodes. To do this, we used the "Emotion" task from the HCP battery of fMRI experiments, in which participants performed a matching task using images of faces or shapes. We contrasted activation in face versus shape blocks and reviewed the results at the whole-brain group level across all 622 participants, $p < .05$ FWE (see **Fig. 4**). This revealed a network of significant BOLD clusters spread across occipital, temporal, frontal, parietal, and subcortical areas, replicating previous work with this dataset[28]. Critically, the most significant cluster included the left and right amygdala as well as the left and right fusiform gyri (FG) and inferior occipital gyri (IOG). These latter two regions are key nodes in the cortical visual processing stream for faces, which may feed information forward to the amygdala[2].

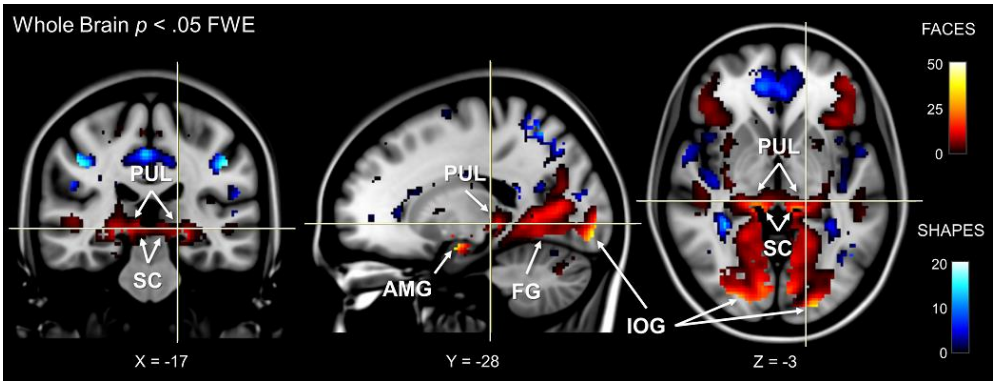

Figure 4. **Whole-brain fMRI activation for faces and shapes.** Face activation is shown by hot colours and shape activation is shown by cool colours. MNI coordinates are shown at the bottom. Labels indicate significant ($p < .05$, whole brain FWE) activation in the superior colliculus (SC), pulvinar (PUL), amygdala (AMG), inferior occipital gyrus (IOG), and fusiform gyrus (FG). Results are overlayed on an averaged MNI152 T1 template.

We used the SPM Anatomy Toolbox to confirm the anatomical positions of our functional activations. In the absence of an anatomical template for the superior colliculus and the pulvinar, we masked the map of statistically significant voxels ($p < .05$, FWE) with our *a priori* manual anatomically-defined superior colliculi mask and functionally-defined pulvinar masks from Barron et al. (2015; see **Online Methods** for ROI generation). This revealed significant voxels in each area (proportion of significant voxels within each mask: left SC = 65.08%, right SC = 73.55%, left PUL = 36.13%, right PUL = 51.49%). Therefore, the "Emotion" HCP task established functional activation in the three subcortical nodes of interest, as well as two nodes of a potential cortical pathway to the amygdala for conveying information about emotional faces.

A forwards-only subcortical route is engaged during face processing

After observing significant BOLD signal in regions along the subcortical route as well as in other visual cortical areas, we next asked whether these regions were dynamically connected. We designed a space of testable models that mapped onto the functional hypothesis of a subcortical route to the amygdala that operates alongside a cortical visual pathway and is modulated by faces. Due to the presence of the IOG and FG in the whole-brain correct fMRI activation and their known roles in face processing[29], we defined several plausible functional cortical connections to the amygdala. These consisted of reciprocal pathways between IOG and FG, FG and amygdala, IOG and amygdala, as well as pulvinar and IOG (see **Fig. 5**). We named models containing both a cortical and subcortical route to the amygdala as “Dual” models, whereas models in which the subcortical route was absent were named “Cortical”. Our model space also included different sources of visual input, namely to the superior colliculus, pulvinar, or both, given that the pulvinar also receives direct retinal input 30 as well as input via the superior colliculus31. This gave us six families of models: 1) Cortical with SC input, 2) Cortical with PUL input, 3) Cortical with SC and PUL input, 4) Dual with SC input, 5) Dual with PUL input, and 6) Dual with SC and PUL input. We considered all possible combinations of forwards and reciprocal (forwards and backwards) cortical and subcortical connections, giving us a comprehensive model space of 102 models.

Of the available 622 participants, we conducted dynamic causal modelling on a subset of 237 participants who had sufficient above-threshold activation in all ROIs (these were defined by the subcortical masks used thus far and by spheres surrounding the coordinate of peak group BOLD signal in the IOG and FG; see Online Methods for more details). We conducted Bayesian model selection on the model space (grouped by families) to estimate how well the models explained the data, taking into account model complexity. We used the random effects implementation to account for potential individual differences in the recruitment of a subcortical pathway for viewing faces32. The winning family was the "Dual with SC and PUL input" family (expected probability = 67.34%, exceedance probability = 100%) and the winning model across the

entire model space was also within this family (expected probability = 21.24%, exceedance probability = 98.01%, protected exceedance probability = 98.18%; see **Fig. 5**). This model included reciprocal cortical connections between IOG and FG and between FG and the amygdala. It also included a forwards-only subcortical route from the superior colliculus to the pulvinar to the amygdala, with input to both the superior colliculus and the pulvinar. The Bayesian Omnibus Risk score was P =1.78 x 10^{-124}, indicating a very small chance that the winning model was indistinguishable from all models tested[33]. We replicated this finding (same winning family and winning model) on a subsample consisting of only the unrelated (i.e. non-sibling) participants within this group (49 participants; see **Supplementary materials**).

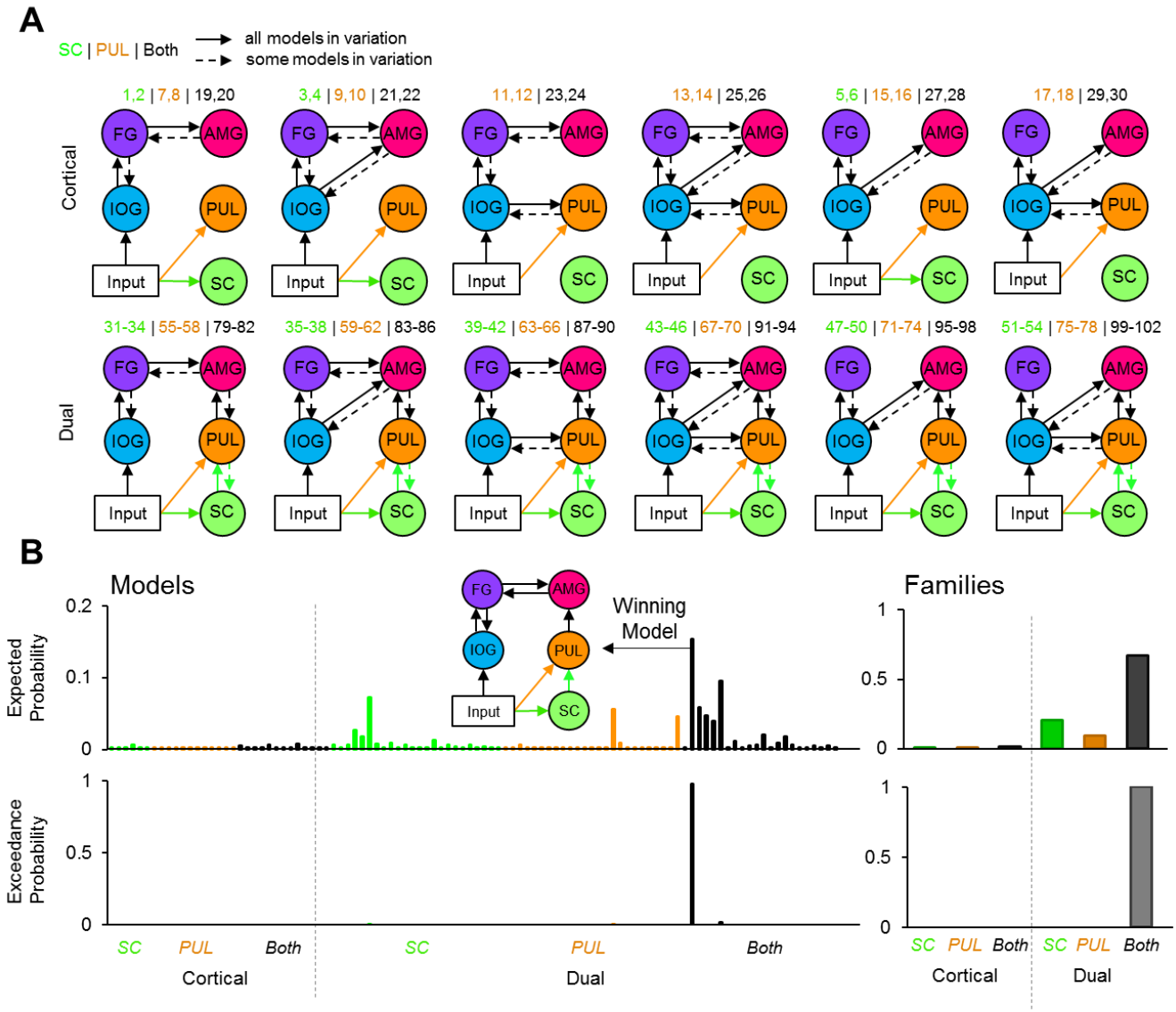

Figure 5. **Dynamic causal modelling model space and estimated probabilities. A)** Diagram of the model space constructed for the fMRI activation to viewing faces. The top row shows various types of model designs in the Cortical family, and the bottom row shows model designs in the Dual family (which includes a subcortical route). Each model variation included different combinations of forwards and backwards connections, indicated by dashed arrows. The model numbers are shown above each model variation. Every model contained input to the inferior occipital gyrus but some models also contained input to the superior colliculus (green) only, pulvinar (orange) only, or both (black). **B)** The expected (top row) probabilities and exceedance probabilities (bottom row) for each of the 102 models. The colour of the bars indicates the different type of input for that family (i.e., SC, PUL, or both), according to A). Individual model probabilities are shown on the left (including a diagram of the winning model) and the probabilities for the families are shown on the right.

The winning model revealed that the functional network that best explained the fMRI activity in our sample of 237 participants included visual inputs to the superior colliculus and pulvinar, forward connections from superior colliculus to the amygdala via the pulvinar, and recurrent interactions between IOG and FG, as well as between FG and amygdala. To extrapolate this finding to the general population and assess the consistency of dynamic coupling at each individual connection, we performed inferential statistics (*t*-tests) on the parameter estimates of each connection within the winning model (i.e. connectivity strength, in their natural space). We looked at the connectivity modulation parameters that represent the change in connection strength caused by the effect of faces. We removed extreme outliers (>3 SDs from mean) participants from each connection ($M = 5.25$, range = 3 to 8 participants excluded) and found that all connectivity modulations were significant except for the backward connection from left and right FG to left IOG (see **Fig. 6**). These results suggest that the modulation of these connections by faces was consistently strong and so we can infer that a subcortical route for processing faces is likely present within the general population.

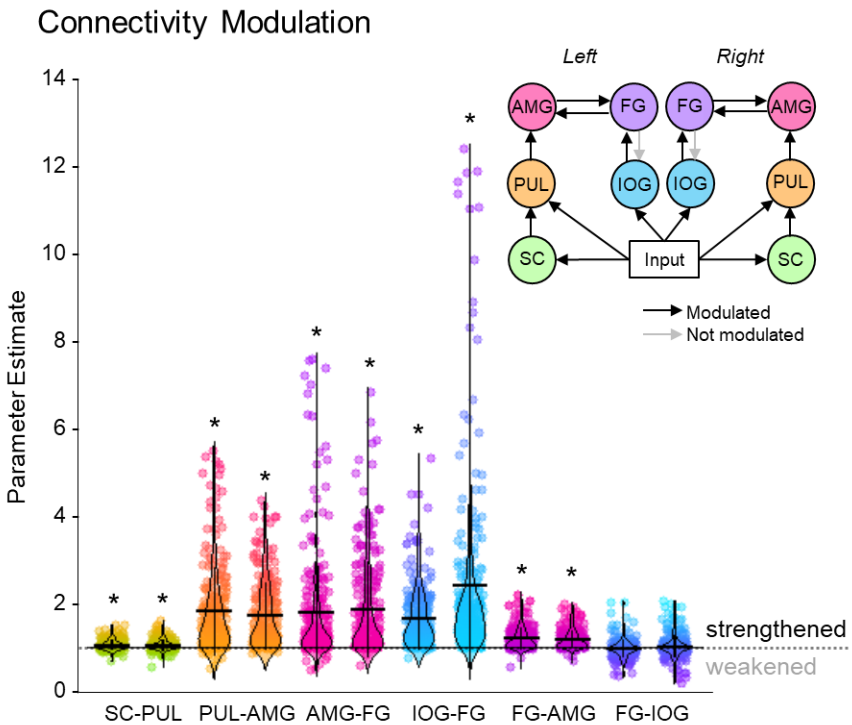

Figure 6. **The strength of individual connections from the winning dynamic causal model.** Parameter estimates of the modulatory connection strength of the winning model. Dot plots of up to 237 participants are shown with horizontal lines for the mean and vertical lines for one standard deviation. Density distribution is represented by each violin plot. The long horizontal dotted line across the graph represents the prior (set to 1), where * indicates the connection was significantly greater than 1 ($p < .05$, corrected for multiple comparisons). A diagram of the winning model (left and right hemispheres are shown) is at the top right. Greyed-out connections indicate those that were not significant.

Greater fibre density relates to stronger effective connectivity

Our findings from tractography, fMRI, and dynamic causal modelling provide convergent evidence for a subcortical route to the amygdala in humans. The final question we set out to answer was whether this converging evidence was correlated, such that participants with stronger structural connectivity also had stronger effective connectivity. In other words, we asked whether the structural connectivity along the subcortical amygdala route enables functional interactions amongst the nodes that lie within it. We computed eight correlations to examine the relationship between each parameter estimate and the corresponding global fibre count and local summed weights per connection (left and right SC-PUL and PUL-AMG). After removing outliers from each pairing according to Cook's Distance (threshold = 3 SDs from the mean), we discovered that participants with more global fibres also had greater modulatory activity for the right PUL-AMG connection ($r = .200$, $p_{bonf} = .023$, N = 220; see **Fig. 7**). We successfully replicated

this finding within a subsample of unrelated participants (49 participants; see **Supplementary Materials**). Thus, our study is the first to successfully harmonise functional and structural information about the subcortical route to the amygdala.

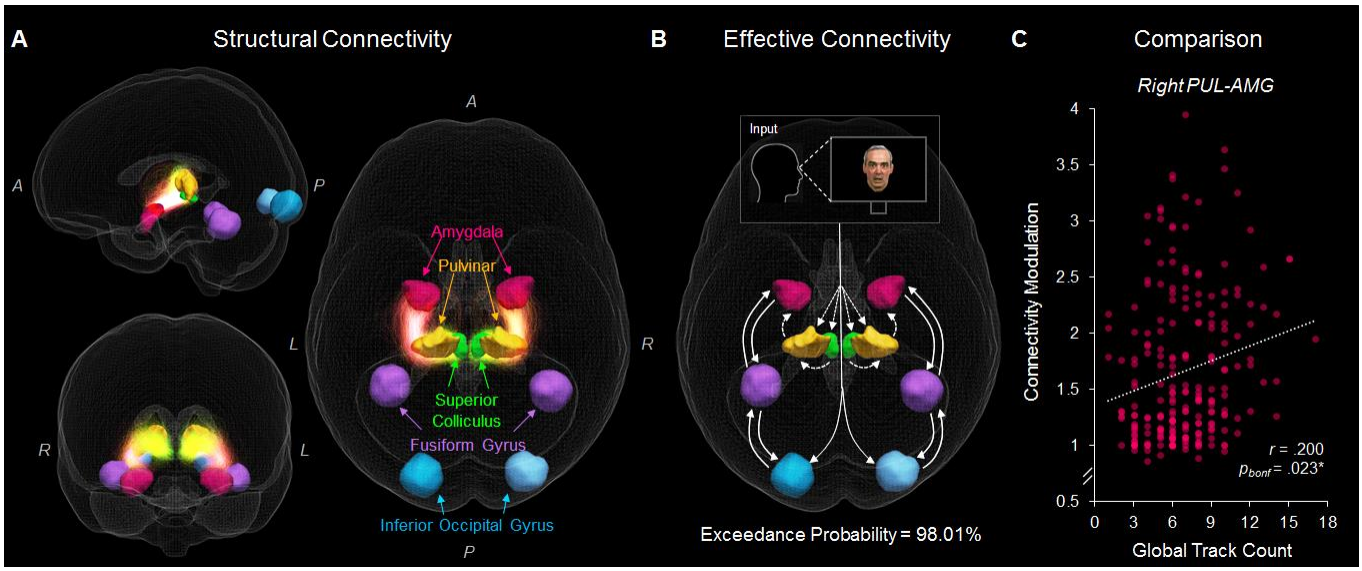

Figure 7. The relationship between structural and effective connectivity for the subcortical route. A and **B** show 3D renders of the ROIs used in the dynamic causal modelling stage. A = anterior, P = posterior, R = right, L = left. **A)** 3D-rendered tracks generated by global tractography overlaid for all 622 participants (pink/orange for PUL-AMG, green/yellow for SC-PUL). Sagittal (top left), coronal (bottom left), and axial (right) views are shown. **B)** direction of information flow according to the winning dynamic causal model (exceedance probability = 98.01%) illustrated using an axial view of the network. Dotted lines indicate subcortical input/connections. **C)** positive correlation between global track count for the right PUL-AMG connection and the modulatory strength of the same connection in the winning effective connectivity model.

Discussion

The elusive subcortical route to the amygdala has posed a unique challenge in studies of the human brain, due to its depth and its rapid, short-lived activity. Evidence has accumulated over recent years across many studies using various neuroimaging modalities showing that this pathway may underlie primitive threat-related behaviour. These studies, however, often take a unimodal approach on typically small samples, making it difficult to relate the specific structural connections between superior colliculus, pulvinar, and amygdala to observed functional brain activity and behavioural output. Our study, which used a large sample of participants from the HCP, unequivocally supports the existence of a subcortical route to the amygdala via the pulvinar in the healthy human adult brain that facilitates dynamic coupling between these regions and enhances fear recognition. We reconstructed the subcortical route to the amygdala using sophisticated tractography methods and found that the white matter fibre density significantly predicted individuals' ability to recognise fearful faces. We then computationally modelled the functional neural networks along this structurally connected network that were engaged while people viewed emotional faces. We found that it was far more likely for the network to include a subcortical visual route to the amygdala than a cortical route alone. Finally, we revealed converging evidence from structural and effectivity connectivity, such that the fibre density of the right pulvinar to amygdala pathway was positively correlated with the strength of the dynamic coupling (i.e. effective connectivity) between these regions.

This study marks the first time that structural and effective connectivity have been concurrently investigated in the one, large sample to address the controversy on the existence and functional role of the putative subcortical route to the amygdala. Tractography of diffusion images is susceptible to both false positives

and false negatives and thus is seldom used in isolation to determine the existence of particular neuroanatomical pathways[34]. We established the validity of our tractographically-reconstructed subcortical route by directly relating our measures of fibre density to both behaviour and effective connectivity, as well as by using two different tractography methods. Had the fibre density measures been simply due to noise, we would not have expected these theoretically relevant relationships with fearful face processing to emerge within this large sample of individuals. Our findings reconcile the long-debated question of whether a pathway from the superior colliculus to the pulvinar to the amygdala is anatomically present and functionally involved in processing visual threat information in humans[14, 15, 35].

Another disputed feature of the subcortical route is its continuity, given discrepancies in the animal literature between which pulvinar subregions connect to the superior colliculus and the amygdala[15]. We provide new evidence that the right inferior pulvinar may mediate direct communication between the superior colliculus and the amygdala in the human brain, building upon previous animal research[31, 36-38]. Moreover, our results show that only the connection from the pulvinar to the amygdala is specifically related to fearful face processing. This suggests a central role for the pulvinar in processing emotional faces, as has been found by previous studies in the macaque[11, 39]. We did not exhaustively explore the extent to which the cortex contributes information to the pulvinar-amygdala connection. The winning effective connectivity model, however, did not include cortical connections between the pulvinar and the inferior occipital gyrus or fusiform gyrus. Hence, it is unlikely that these cortical visual areas contribute to the information transmitted along the subcortical route. It remains to be shown how interactions between the pulvinar and other cortical areas, such as the inferotemporal cortex[17], may influence activity along the pulvinar-amygdala connection.

Our findings open avenues for future studies on how this subcortical pathway might influence threat-related behaviour. Recent research has revealed that the superior colliculus, pulvinar, and amygdala show greater BOLD signal when individuals with autism fixate on the eyes of a face, more so than controls[40]. Future studies might therefore explore how the fibre density of this pathway differs in autistic populations. Furthermore, the propensity for the subcortical route to increase pre-attentive[41] or unconscious[2] processing of threatening stimuli might play a significant and relatively unexplored role in anxiety disorders, such as social anxiety and post-traumatic stress disorder.

In conclusion, our study settles a long-held debate over the existence and function of a subcortical route to the amygdala in the human brain. Our multimodal neuroimaging approach, leveraged by computational modelling, provides convergent evidence for a fundamental and conserved pulvinar-amygdala pathway that is specifically involved in fear. We demonstrate that the white matter tracts that form the subcortical structural pathway from the pulvinar to the amygdala enables functional, dynamic interactions amongst the regions that lie within it. Critically, we show that structural connectivity between the pulvinar and the amygdala leads to better recognition of fearful expressions in human faces.

Online methods

Participants

We used the data from the publicly available Human Connectome Project (HCP) S900 release, collected between 2012 and 2016[24]. The S900 release contained 730 young adults with complete MRI and dMRI data, as well as fMRI data for the emotion task[42]. Of these, we excluded 95 people due to positive drug/alcohol tests and an additional 13 for abnormal colour vision. This resulted in a final sample of 622 participants aged between 22 and 36 years (M = 28.81, SD = 3.68 years), 259 of whom were male and 363 female, with 569 right-handed and 53 left-handed. Within our sample, 495 participants were related to one or more other participants (328 families in total). This included 53 pairs of monozygotic twins, 50 pairs of dizygotic twins,

and 289 participants with one or more non-twin siblings in the sample. The remaining 127 participants were unrelated. We acknowledged that the many siblings in the HCP sample might spuriously decrease the variance in our neural measures (due to the structural and functional similarity between siblings, for example) and thus influence our statistics. Because of this, we replicated some of the analyses from the full sample on the subsample of unrelated participants (see **Supplementary Materials**).

dMRI Processing

dMRI Acquisition

The HCP scanned participants in sessions over two days using a custom-made Siemens 3T "Connectome Skyra" (Siemens, Erlangen, Germany) with a 32-channel head coil, located at Washington University, St Louis, USA. They collected two separate T1-weighted high-resolution MPRAGE images (voxel size = 0.7mm isotropic, field of view = 224mm, matrix = 320, 256 saggital slices, TR = 2,400ms, TE = 2.14ms, TI = 1,000ms, flip angle = 8°, bandwidth = 210Hz per pixel, echo spacing = 7.6ms). We only used the first T1 image of the two sessions in our analysis. The HCP collected multi-band multi-shell diffusion-weighted images in a single session also using the Connectome Skyra (3 shells with b-values of 1000, 2000, and 3000 s/mm^2; 90 directions per shell; voxel size = 1.25mm isotropic; TR = 5520ms; TE = 89.5ms; flip angle = 78°; field of view = 210 x 180mm; refocusing flip angle = 160°; echo spacing = 0.78ms; bandwidth = 1488 Hz/pixel; slice thickness = 111 x 1.25mm).

dMRI Preprocessing

We used the minimally processed images provided by the HCP. For the T1 images, this included gradient distortion correction, bias field correction (using FSL: Jenkinson, Beckmann, Behrens, Woolrich, & Smith, 2012; http://fsl.fmrib.ox.ac.uk/fsl/fslwiki/), and cortical segmentation (using FreeSurfer: Dale, Fischl, & Sereno, 1999; http://surfer.nmr.mgh.harvard.edu/). For the diffusion images, this included intensity normalisation across runs, echo planar imaging (EPI) distortion correction and eddy current/motion correction (for full details, see Glasser et al. 2013). We conducted all further processing using MRTrix 3.0.15[44] and FSL 5.0.7.

Global Intensity Normalisation

First, we corrected for low-frequency B1 field inhomogeneities in the dMRI volumes. We then conducted global intensity normalisation across each participant's corrected diffusion-weighted image so that we could later perform quantitative analyses of fibre density (i.e. apparent fibre density[45]). This step normalises the median white matter b=0 intensity (i.e. non-diffusion-weighted image) across participants so that the proportion of one tissue type within a voxel does not influence the diffusion-weighted signal in another. Given our large sample size, we selected a subset of 62 participants (approximately 10% of the sample) to create a representative fractional anisotropy (FA) population template and white matter mask. We then used the population template and white matter mask to normalise the white matter intensity of all 622 participants' dMRI volumes.

Response Function Estimation

We segmented each participant's T1 image into five tissue types (cortical grey matter, subcortical grey matter, white matter, CSF, and pathological tissue) using the Freesurfer parcellation image provided by the HCP. We then estimated response functions (i.e. the signal expected for a voxel containing a single, coherently-oriented fibre bundle) for grey matter, white matter, and CSF using the Multi-Shell Multi-Tissue (MSMT) Constrained Spherical Deconvolution (CSD) algorithm[46]. After completing this step for all participants, we averaged their response functions to produce representative response functions per tissue

type. We then conducted MSMT CSD on each participant again using the group averaged response functions, producing individual multi-tissue fibre orientation distributions (FODs).

fMRI Processing

fMRI Acquisition

As with the dMRI data, the HCP acquired whole-brain gradient-echo echo planar imaging (EPI) data using the Connectome Skyra (TR = 720ms, TE = 33.1ms, flip angle = 52°, bandwidth = 2,290 Hz/Px, in-plane field of view = 208 x 180mm, 72 slices at 2mm thick, voxel size = 2mm isotropic, echo spacing = 0.58ms) with a multiband factor of eight. They collected data in a one-hour session (either on the same day as the dMRI or one day before/after) along with two or three other functional tasks in the HCP battery. For the emotion task, there were two runs, one with right-to-left phase encoding and the other with left-to-right phase encoding, each with 176 frames at a duration of 2 minutes and 16 seconds.

fMRI Task

The HCP developed the "emotion task" from the paradigm presented by Hariri, Mattay, Tessitore, Kolachana, Fera, Goldman, Egan and Weinberger [47]. Participants were presented with three visual stimuli at a time (one image at the top and two at the bottom) using E-Prime[48]. Participants were then instructed to make a button press indicating which of the two images at the bottom (left or right) matched the image at the top. Images were either a face (angry or fearful) or a shape (circle, horizontal oval, or vertical oval). The stimuli were presented on screen for 2,000ms separated by a 1,000ms inter-stimulus interval. A cue was presented at the beginning of each block to indicate the block type (i.e. “shape” or “face”), where each block contained either 6 faces trials or 6 shapes trials. Finally, a fixation cross was presented for eight seconds at the end of each of each run. The last block of each run only contained the first three trials due to a technical error that occurred early in HCP data collection. As the first block was always a shape block, our analysis was conducted on three shape blocks and 2.5 face blocks.

fMRI Preprocessing

We used the minimally preprocessed fMRI data provided by the HCP corrected for gradient distortion, motion, and field map-based EPI distortion. The HCP intensity normalised the data and spatially transformed it to MNI152 space using FSL (see Glasser et al. 2013 for full details on preprocessing pipeline). We further increased the signal-to-noise ratio of the fMRI data in SPM12 (SPM12, www.fil.ion.ucl.ac.uk/spm) by applying spatial smoothing using a 4mm Gaussian kernel[49].

Regions of Interest

We chose the superior colliculus, pulvinar, and amygdala as our ROIs We created masks of these ROIs in standard MNI space using FSL. For the amygdala (AMG) mask, we used the probabilistic Harvard-Oxford Subcortical atlas at a threshold of at least 50% probability. For the pulvinar (PUL), we were interested in the structure as a whole, as well as its subregions. To do this, we used the parcellated pulvinar mask generated by Baron et al. (2015), who isolated five distinct pulvinar clusters based on functional co-activation profiles in fMRI data from 29,597 participants across 7,772 experiments[12]. For the pulvinar as a whole ROI, we merged the five clusters together and used FSL to manually fill any holes in the resultant mask. Finally, we manually created masks for the left and right superior colliculi (SC) in the absence of an atlas-based mask by drawing the boundaries of the superior colliculus over the MNI152 single participant T1 template with reference to an anatomical atlas[50] and filling the centre. We then used FSL to warp these masks into native diffusion space for each participant's tractography analysis. All our ROIs in MNI space are freely available online from the Open Science Framework: doi:10.17605/OSF.IO/KBPWM.

dMRI analysis

In this study, we implemented two tractography methods that use different approaches to white matter reconstruction for cross-method validation. We first used the multi-tissue model of global tractography. This method takes a Bayesian approach to reconstructing a full-brain fibre configuration using a generative signal model to best explain the underlying data. It is less sensitive to noise that may accumulate for longer distance tracts in other "local" tractography methods throughout their stepwise approach[51, 52]. Hence, for comparison, we computed probabilistic tractography between our regions of interest[53]. This method also uses a Bayesian approach to account for one or more distributions of fibre orientations within each voxel, thus incorporating uncertainty into the model[54]. To acquire a biologically-accurate measure of apparent fibre density[45] along the resultant streamlines, we used the Spherical-Deconvolution Informed Filtering of Tractograms version 2 (SIFT2) method to weight each streamline by a cross-sectional area multiplier directly related to the underlying data[26, 45].

Global tractography

Global tractography is a data-driven Bayesian approach to estimating the whole-brain fibre configuration that best explains the underlying diffusion-weighted images. As opposed to local streamline tracking, global tractography accounts for the spatial continuity of fibres and thus is better able to discriminate crossing and fanning fibre geometries[51]. Furthermore, because the simultaneously-reconstructed fibre configurations are optimised with respect to the data at hand, the density of the final tractogram quantitatively represents the apparent fibre density (AFD; i.e. the proportion of space occupied by white matter fibres[45]).

We conducted global tractography on the global-intensity-normalised DWI volumes for each participant using the group-averaged multi-tissue response functions. After 250 million iterations to optimise a full brain reconstruction, we filtered the tractogram using the ROI masks described above to isolate fibres that terminated in 1) both the superior colliculus and pulvinar masks, and 2) both the pulvinar and amygdala masks. We also used the masks for the five individual functionally-defined pulvinar subregions to isolate the subregion-specific fibres connecting to the superior colliculus and to the amygdala. Before any statistical analysis, we removed four participants with extreme values more than 3 SDs from the mean of all connections, as these likely indicated artefactual imaging data (final N = 618). These outliers were also removed from the pulvinar subregion-specific analyses.

Local tractography

As a less conservative approach than global tractography, we also conducted local probabilistic tractography using our ROIs as seeding and terminating regions. We used the iFOD2 algorithm, iteratively planting a seed point 25,000 times (or until at least 10,000 tracks had been selected and written) in each voxel of the seeding ROI[44]. We applied the anatomically-constrained variation of this technique, whereby each participant's five-tissue-type segmented T1 image provided biologically-realistic priors for streamline generation, reducing the likelihood of false positives[55]. We edited the final streamlines so that only those that terminated in our ROIs remained.

Using these methods, we traced streamlines between the two halves of the subcortical route (i.e. SC to PUL, PUL to AMG). We then reversed the seeding location (i.e. PUL to SC, AMG to PUL) and based all statistics on the average between the forwards and backwards seeding directions to reduce any influence of possible asymmetries in seed ROI volume. We applied SIFT2 to these streamlines to enable us to quantitatively assess the connectivity. SIFT2 makes this possible by weighting the streamlines by a cross-sectional multiplier such that the sum of these weighting factors better represents the underlying white matter fibre density[55]. Before computing any statistics, we removed 13 participants whose average summed weights

across each connection were more than 3 SDs from the mean (final N = 609). These outliers were also absent from the pulvinars subregion-specific analyses.

Pulvinar subregion analysis

We were interested in which of the subregion-specific pathways between the superior colliculus and the pulvinar correlated with those between the amygdala and pulvinar. We constructed correlation matrices with 5 subregion SC-PUL variables on one axis and 5 subregion PUL-AMG variables on the other. This was done per hemisphere and per local/global tractography method (see **Fig. 2**). The SC-PUL variables and PUL-AMG variables were highly intercorrelated within each set, meaning that any relationship between an SC-PUL subregion and PUL-AMG subregion would be strongly influenced by other SC-PUL subregions. To isolate the unshared variance of each subregion-specific pathway, we performed principal components analysis (using Varimax rotation orthogonalise the variables) to specifically extract five components. Bartlett's test of sphericity was significant for each analysis and the minimum Kaiser-Meyer-Olkin measure of sampling adequacy was at least .696 for global tractography and .687 for local tractography.

fMRI analysis

General linear modelling

Using the spatially smoothed fMRI data, we convolved the onset of each Face and Shape block with a canonical hemodynamic response function (HRF) using SPM12. We closely modelled this first-level general linear model (GLM) analysis on the work by Hillebrandt et al., (2014), such that we did not slice time correct the multiband data due to the fast TR. We partitioned the GLM into sessions (left-to-right and right-to-left encoding) and we included head motion as a regressor. We generated statistical parametric maps (SPMs) of the expected BOLD signal for faces minus shapes and shapes minus faces.

We then entered the faces minus shapes contrast into a second-level analysis (a one-sample *t*-test) across all participants. After examining the estimated BOLD signal to Faces at the whole-brain level ($p < .05$, family-wise error corrected using Random Field Theory[11]), we applied the superior colliculus, pulvinar, and amygdala *a priori* defined masks to more specifically estimate functional activation in these anatomically-defined areas.

Dynamic causal modelling

We implemented Dynamic Causal Modelling (DCM) to infer the causal direction of information flow between neural regions using a biophysically informed generative model[56]. First, we examined the map of significant activation produced by the fMRI analysis of the "Emotion" HCP task. Based on this and our *a priori* hypotheses, we defined the left and right superior colliculus, pulvinar, amygdala, inferior occipital gyrus (IOG), and fusiform gyrus (FG) as our ROIs. For the two gyri, we used MNI coordinates of the most significant peak from the group level analysis (left IOG: -22 -92 -10, right IOG: 28 -90 -8, left FG: -38 -50 -20, right FG: 40 -52 -18). We then placed spheres with a radius of 12mm around these four coordinates to search for the participant-specific local maxima within each participant's session-specific SPM for the faces minus shapes contrast (adjusted for the *t* effects of interest, $p < .05$ uncorrected). Note that for the purposes of extracting the fMRI data for the DCM nodes, one does not need corrected p-values [49]. Next, we defined the ROIs by a 6mm radius sphere around the participant- and session- specific local maxima. For the subcortical areas of interest, we defined the initial search radius by the anatomically defined ROI masks (as described above) instead of significant peaks from the group analysis to confine our search within subcortical grey matter.

We used a "two-state" DCM model, which accounts for both excitatory and inhibitory neural populations[49, 57]. Our model space was dictated by our specific, theory-driven hypotheses about subcortical and cortical visual pathways to the amygdala, as well as by the significant regions of the BOLD signal observed at the group level in our GLM analysis. Both face and shape blocks contributed to input parameters within each model. All endogenous and intrinsic connections in each model were modulated by the effect of faces over shapes.

To specify a DCM, each participant needed to have above-threshold activation (at $p < .05$, uncorrected) within each ROI across both scanning sessions. This was the case for 237 out of the 622 participants. The ROIs with the lowest number of above-threshold participants were the left and right superior colliculi (69 and 58 participants, respectively), followed by the left and right pulvinar (4 and 3 participants, respectively). This may be due to the bilateral superior colliculi's relatively smaller volume as well as lower statistical power (its mean *t*-statistic was approximately 10.57 compared with 33.35 for IOG and 30.14 for FG). Critically, the 237 participants with above-threshold activity in all ROIs did not differ significantly from the other 385 participants in the global or local tractography results, performance on the Penn Emotion Recognition task, volume of the thalamus/amygdala/fusiform area/lateral occipital area (as computed by Freesurfer), reaction time/accuracy to faces/shapes during the fMRI task, age, or gender. Therefore, using the information available to us, we had no evidence to assume that our DCM sample was biased by any confounding variable.

The final model space consisted of 102 models (see **Fig. 5**), where the first Cortical family contained six models, the second and third Cortical families contained 12 models each, and the Dual families (families 4, 5, and 6) contained 24 models each. The different families correspond to different input types (superior colliculus only, pulvinar only, or superior colliculus and pulvinar) and the different models within these families arise from different combinations of forward and backward connections. Each of the final 102 DCMs were modelled separately for both fMRI sessions. Both hemispheres were included in each model with no cross-hemispheric connections.

References

1. LeDoux, J. The emotional brain: The mysterious underpinnings of emotional life. *Simon and Schuster* (1998).
2. Tamietto, M. & de Gelder, B. Neural bases of the non-conscious perception of emotional signals. *Nature Reviews Neuroscience* **11**, 697-709 (2010).
3. Morris, J.S., Öhman, A. & Dolan, R.J. A subcortical pathway to the right amygdala mediating "unseen" fear. *Proceedings of the National Academy of Sciences* **96**, 1680-1685 (1999).
4. Gerbella, M., Caruana, F. & Rizzolatti, G. Pathways for smiling, disgust and fear recognition in blindsight patients. *Neuropsychologia* (2017).
5. Pegna, A.J., Khateb, A., Lazeyras, F. & Seghier, M.L. Discriminating emotional faces without primary visual cortices involves the right amygdala. *Nature Neuroscience* **8** (2005).
6. Vuilleumier, P., Armony, J.L., Driver, J. & Dolan, R.J. Distinct spatial frequency sensitivities for processing faces and emotional expressions. *Nature Neuroscience* **6**, 624-631 (2003).
7. Liddell, B.J., *et al.* A direct brainstem–amygdala–cortical 'alarm' system for subliminal signals of fear. *NeuroImage* **24**, 235-243 (2005).
8. McFadyen, J., Mermillod, M., Mattingley, J.B., Halász, V. & Garrido, M.I. A Rapid Subcortical Amygdala Route for Faces Irrespective of Spatial Frequency and Emotion. *The Journal of Neuroscience* **37**, 3864-3874 (2017).
9. Garvert, M.M., Friston, K.J., Dolan, R.J. & Garrido, M.I. Subcortical amygdala pathways enable rapid face processing. *NeuroImage* **102**, 309-316 (2014).

10. Rudrauf, D., *et al.* Rapid Interactions between the Ventral Visual Stream and Emotion-Related Structures Rely on a Two-Pathway Architecture. *The Journal of Neuroscience* **28**, 2793-2803 (2008).
11. Soares, S.C., Maior, R.S., Isbell, L.A., Tomaz, C. & Nishijo, H. Fast Detector/First Responder: Interactions between the Superior Colliculus-Pulvinar Pathway and Stimuli Relevant to Primates. *Frontiers in Neuroscience* **11** (2017).
12. Barron, D.S., Eickhoff, S.B., Clos, M. & Fox, P.T. Human pulvinar functional organization and connectivity. *Human Brain Mapping* **36**, 2417-2431 (2015).
13. Koller, K., Rafal, R.D., Platt, A. & Mitchell, N.D. Orienting toward threat: Contributions of a subcortical pathway transmitting retinal afferents to the amygdala via the superior colliculus and pulvinar. *Neuropsychologia* (2018).
14. Pessoa, L. & Adolphs, R. Emotion processing and the amygdala: from a 'low road' to 'many roads' of evaluating biological significance. *Nature Reviews Neuroscience* **11**, 773-783 (2010).
15. Pessoa, L. & Adolphs, R. Emotion and the brain: multiple roads are better than one. *Nature Reviews Neuroscience* **12**, 425-425 (2011).
16. Bridge, H., Leopold, D.A. & Bourne, J.A. Adaptive Pulvinar Circuitry Supports Visual Cognition. *Trends in Cognitive Sciences* **20**, 146-157 (2016).
17. Zhou, H., Schafer, R. & Desimone, R. Pulvinar-Cortex Interactions in Vision and Attention. *Neuron* **89**, 209-220 (2016).
18. Zhou, N.A., Maire, I.S., Terson, S.P. & Bickford, M.E. The mouse pulvinar nucleus: Organization of the tectorecipient zones. *Visual Neuroscience* **34** (2017).
19. Wei, P., *et al.* Processing of visually evoked innate fear by a non-canonical thalamic pathway. *Nature Communications* **6** (2015).
20. Shang, C., *et al.* A parvalbumin-positive excitatory visual pathway to trigger fear responses in mice. *Science* **348**, 1472-1477 (2015).
21. Tamietto, M., Pullens, P., de Gelder, B., Weiskrantz, L. & Goebel, R. Subcortical connections to human amygdala and changes following destruction of the visual cortex. *Current biology : CB* **22**, 1449-1455 (2012).
22. Rafal, R.D., *et al.* Connectivity between the superior colliculus and the amygdala in humans and macaque monkeys: virtual dissection with probabilistic DTI tractography. *Journal of Neurophysiology* **114**, 1947-1962 (2015).
23. Silverstein, D.N. & Ingvar, M. A multi-pathway hypothesis for human visual fear signaling. *Frontiers in Systems Neuroscience* **9**, 101 (2015).
24. Van Essen, D.C., *et al.* The WU-Minn Human Connectome Project: an overview. *NeuroImage* **80**, 62-79 (2013).
25. Morris, D.M., Embleton, K.V. & Parker, G. Probabilistic fibre tracking: Differentiation of connections from chance events. *NeuroImage* **42**, 1329-1339 (2008).
26. Smith, R.E., Tournier, J.-D., Calamante, F. & Connelly, A. SIFT2: Enabling dense quantitative assessment of brain white matter connectivity using streamlines tractography. *NeuroImage* **119**, 338-351 (2015).
27. Morel, A., Magnin, M. & Jeanmonod, D. Multiarchitectonic and stereotactic atlas of the human thalamus. *Journal of Comparative Neurology* **387**, 588-630 (1997).
28. Barch, D.M., *et al.* Function in the human connectome: Task-fMRI and individual differences in behavior. *NeuroImage* **80**, 169-189 (2013).
29. Johnson, M.H. Subcortical face processing. *Nature Reviews Neuroscience* **6**, 766-774 (2005).
30. Cowey, A., Stoerig, P. & Bannister, M. Retinal ganglion cells labelled from the pulvinar nucleus in macaque monkeys. *Neuroscience* **61**, 691-705 (1994).
31. Berman, R.A. & Wurtz, R.H. Signals Conveyed in the Pulvinar Pathway from Superior Colliculus to Cortical Area MT. *The Journal of Neuroscience* **31**, 373-384 (2011).

32. Stephan, K.E., Penny, W.D., Daunizeau, J., Moran, R.J. & Friston, K.J. Bayesian Model Selection for Group Studies. *NeuroImage* **47** (2009).
33. Rigoux, L., Stephan, K.E., Friston, K.J. & Daunizeau, J. Bayesian model selection for group studies — Revisited. *NeuroImage* **84**, 971-985 (2014).
34. Jbabdi, S. & Johansen-Berg, H. Tractography: Where Do We Go from Here? *Brain Connectivity* **1**, 169-183 (2011).
35. de Gelder, B., van Honk, J. & Tamietto, M. Emotion in the brain: of low roads, high roads and roads less travelled. *Nature Reviews Neuroscience* **12**, 425-425 (2011).
36. Stepniewska, I. & Kaas, J.H. Architectonic subdivisions of the inferior pulvinar in New World and Old World monkeys. *Visual Neuroscience* **14**, 1043-1060 (1997).
37. Baldwin, M., Wong, P., Reed, J.L. & Kaas, J.H. Superior colliculus connections with visual thalamus in gray squirrels (Sciurus carolinensis): Evidence for four subdivisions within the pulvinar complex. *Journal of Comparative Neurology* **519**, 1071-1094 (2011).
38. Berman, R.A. & Wurtz, R.H. Functional Identification of a Pulvinar Path from Superior Colliculus to Cortical Area MT. *The Journal of Neuroscience* **30**, 6342-6354 (2010).
39. Maior, R.S., Hori, E., Tomaz, C., Ono, T. & Nishijo, H. The monkey pulvinar neurons differentially respond to emotional expressions of human faces. *Behavioural Brain Research* **215**, 129-135 (2010).
40. Hadjikhani, N., *et al.* Look me in the eyes: constraining gaze in the eye-region provokes abnormally high subcortical activation in autism. *Scientific Reports* **7**, 3163 (2017).
41. Hakamata, Y., *et al.* The functional activity and effective connectivity of pulvinar are modulated by individual differences in threat-related attentional bias. *Scientific Reports* **6**, 34777 (2016).
42. Van Essen, D.C., *et al.* The Human Connectome Project: A data acquisition perspective. *NeuroImage* **62**, 2222-2231 (2012).
43. Glasser, M.F., *et al.* The minimal preprocessing pipelines for the Human Connectome Project. *NeuroImage* **80**, 105-124 (2013).
44. Tournier, J.D., Calamante, F. & Connelly, A. MRtrix: Diffusion tractography in crossing fiber regions. *International Journal of Imaging Systems and Technology* **22**, 53-66 (2012).
45. Raffelt, D., *et al.* Apparent Fibre Density: A novel measure for the analysis of diffusion-weighted magnetic resonance images. *NeuroImage* **59**, 3976-3994 (2012).
46. Jeurissen, B., Tournier, J.-D., Dhollander, T., Connelly, A. & Sijbers, J. Multi-tissue constrained spherical deconvolution for improved analysis of multi-shell diffusion MRI data. *NeuroImage* **103**, 411-426 (2014).
47. Hariri, A.R., *et al.* Serotonin Transporter Genetic Variation and the Response of the Human Amygdala. *Science* **297**, 400-403 (2002).
48. Schneider, W., Eschman, A., Zuccolotto, A. & Burgess, S. E-prime. *Psychology Software Tools* (2002).
49. Hillebrandt, H., Friston, K.J. & Blakemore, S.-J. Effective connectivity during animacy perception - dynamic causal modelling of Human Connectome Project data. *Scientific Reports* **4**, 6240 (2014).
50. Tamraz, J.C. & Comair, Y.G. Atlas of regional anatomy of the brain using MRI. *Springer-Verlag* (2004).
51. Christiaens, D., *et al.* Global tractography of multi-shell diffusion-weighted imaging data using a multi-tissue model. *NeuroImage* **123**, 89-101 (2015).
52. Reisert, M., *et al.* Global fiber reconstruction becomes practical. *NeuroImage* **54**, 955-962 (2011).
53. Tournier, J.D., Calamante, F. & Connelly, A. Improved probabilistic streamlines tractography by 2nd order integration over fibre orientation distributions. *Improved probabilistic streamlines tractography by 2nd order integration over fibre orientation distributions* **1670** (2010).
54. Behrens, T.E.J., Berg, J.H., Jbabdi, S., Rushworth, M.F.S. & Woolrich, M.W. Probabilistic diffusion tractography with multiple fibre orientations: What can we gain? *NeuroImage* **34**, 144-155 (2007).

55. Smith, R.E., Tournier, J.-D., Calamante, F. & Connelly, A. Anatomically-constrained tractography: Improved diffusion MRI streamlines tractography through effective use of anatomical information. *NeuroImage* **62**, 1924-1938 (2012).
56. Friston, K.J., Harrison, L. & Penny, W. Dynamic causal modelling. *Neuroimage* **19**, 1273-1302 (2003).
57. Marreiros, A.C., Kiebel, S.J. & Friston, K.J. Dynamic causal modelling for fMRI: A two-state model. *NeuroImage* **39**, 269-278 (2008).

Acknowledgements

Data were provided by the Human Connectome Project, WU-Minn Consortium (Principal Investigators: David Van Essen and Kamil Ugurbil; 1U54MH091657) funded by the 16 NIH Institutes and Centers that support the NIH Blueprint for Neuroscience Research; and by the McDonnell Center for Systems Neuroscience at Washington University. We would like to thank Dr Anton Lord, Dr Lee Reid, and Professor Klaas Enno Stephan for their valuable help and guidance. This work was funded by a University of Queensland Fellowship (2016000071) to MIG and an Australian Postgraduate Award to JM.

Supplementary materials

Dynamic causal modelling

Within the DCM subsample of 237 participants, 49 were unrelated. For this sample, the winning family was the "Dual with SC and PUL input" (expected probability = 64.86%, exceedance probability = 99.92%). The winning model was within this family (expected probability = 21.15%, exceedance probability = 72.77%) and was the same as the winning model from the full 237 participant sample. Classical statistics on the exponentiated parameter estimates showed that all B parameter estimates were significant except the backward connections between right and left FG to IOG, as was found in the full sample.

We conducted the same series of eight correlations between the structural connectivity measures (global track count and summed weights) and effective connectivity (A and B parameter estimates), while also removing 1 outlier. After correcting for multiple comparisons, we found that participants with greater global fibre count along the right PUL-AMG connection also had stronger modulatory connectivity (r = .422, p_{bonf} = .025) along the same connection.